Inorganic Chemistry

Article

pubs.acs.org/IC

# Mechanism of Photocatalytic Hydrogen Generation by a Polypyridyl-Based Cobalt Catalyst in Aqueous Solution

Alexander Rodenberg, Margherita Orazietti, Benjamin Probst, Cyril Bachmann, Roger Alberto, Kim K. Baldridge, and Peter Hamm*

Department of Chemistry, University of Zürich, Winterthurerstrasse 190, CH-8057 Zürich, Switzerland

Supporting Information

**ABSTRACT:** The mechanism of photocatalytic hydrogen production was studied with a three-component system consisting of *fac*-$[Re(py)(CO)_3bipy]^+$ (py = pyridine, bipy = 2,2′-bipyridine) as photosensitizer, $[Co(TPY\text{-}OH)(OH_2)]^{2+}$ (TPY-OH = 2-bis(2-pyridyl)(hydroxy)methyl-6-pyridylpyridine), a polypyridyl-based cobalt complex, as water reduction catalyst (WRC), and triethanolamine (TEOA) as sacrificial electron donor in aqueous solution. A detailed mechanistic picture is provided, which covers all processes from excited state quenching on the time scale of a few nanoseconds to hydrogen release taking place between seconds and minutes at moderately basic reaction conditions. Altogether these processes span 9 orders of magnitude in time. The following reaction sequence was found to be the dominant pathway for hydrogen generation: After reductive quenching by TEOA, the reduced photosensitizer (PS) transfers an electron to the $Co^{II}$–WRC. Protonation of $Co^{I}$ yields $Co^{III}H$ which is reduced in the presence of excess $Co^{I}$. $Co^{II}H$ releases hydrogen after a second protonation step, which is detected time-resolved by a clark-type hydrogen electrode. Aside from these productive steps, the role of side and back reactions involving TEOA-derived species is assessed, which is particularly relevant in laser flash photolysis measurements with significantly larger transient concentrations of reactive species as compared to continuous photolysis experiments. Most notable is an equilibrium reaction involving $Co^{I}$, which is explained by a nucleophilic addition of $Co^{I}$ to the oxidation product of TEOA, an electrophilic iminium ion. Quantum chemical calculations indicate that the reaction is energetically feasible. The calculated spectra of the adduct are consistent with the spectroscopic observations.

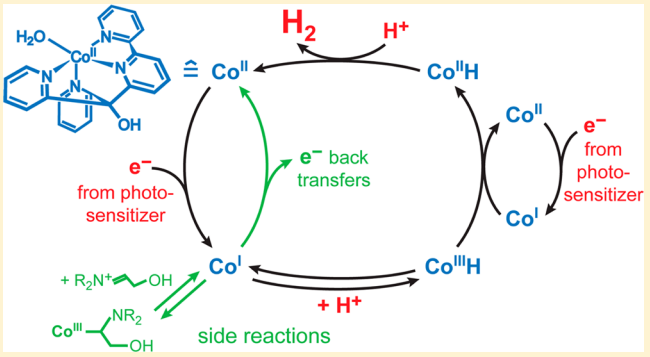


## INTRODUCTION

The ever-growing global demand for fossil fuels, regardless of their limited availability, has triggered tremendous scientific efforts aiming at innovative strategies toward renewable energy sources. One aspect of these efforts is the search for effective and cheap ways to produce chemical fuels, which are easily storable, from solar energy.[1−3] Hydrogen is one prominent potential fuel source, which could be produced directly from water in various ways,[4,5] such as through thermochemical cycling[6−9] and algae,[10−13] as well as electrolysis in combination with photovoltaics and direct photo(electro)chemical methods.[1,14−29] The latter two approaches rely on effective and stable catalysts working at low overpotentials for both water reduction and oxidation. Additionally, a purely aqueous reaction medium is desirable for future upscaling and commercial application. A combination of these properties has been restricted to precious noble metals and their compounds,[30,31] but fast progress with WRCs based on cheap and abundant first-row transition metals has been made over the past decade.[21,24,32−42] The present study aims at contributing to this development by elucidating the mechanism of hydrogen production by a cobalt-based WRC in aqueous solution.

Complexes of cobalt are promising candidates for water reduction. Efforts to implement them into homogeneous water splitting systems date back to the pioneering work of Sutin and Eisenberg on the cobalt macrocycle and cobalt bipyridyl complexes.[43−47] Improved ligand platforms have been developed,[48−54] of which those based on glyoxime[22,55−66] and polypyridyl[67−77] ligands have gained the most attention. Glyoxime derived cobalt WRCs show best performance in organic solvents, such as acetonitrile or DMF and mixtures thereof with varying amounts of water.[24] With balanced pH, catalyst concentrations, and solvent composition, highly optimized photocatalytic systems turnover numbers (TONs) between 700 and 2150 $H_2$/Co have been demonstrated.[55,56,61] Long-term stability is significantly reduced in purely aqueous solution.[57,78] However, many studies use glyoxime type cobalt WRCs because of the ease of their synthesis, low overpotentials typically around 0.2−0.3 V,[24,38] and the ample body of research

**Received:** October 27, 2014
**Published:** December 24, 2014





DOI: 10.1021/ic502591a
*Inorg. Chem.* 2015, 54, 646−657

experience with these catalysts. In contrast, with polypyridyl-based cobalt WRCs, significantly higher TONs (~$10^4$ $H_2$/Co) are achieved in photocatalytic systems in aqueous solution.[69,76,79] The superior long-term performance comes at the cost of typically larger overpotentials around 0.4−0.6 V.[24] Ligand substitutions with electron withdrawing functional groups have been reported to lower the overpotential, however, while simultaneously disminishing catalytic activity.[68−70,79] Current record TONs in photocatalytic systems are achieved only at very low catalyst concentrations, indicating that the photosensitizer stability and the sacrificial donor are the limiting factors. It was recently shown that, in the case of ascorbate as sacrificial donor, the in situ reduction of deteriorating dehydroascorbic acid with tris(2-carboxyethyl)-phosphine increases the maximum TON by a factor of 3, from 11 000 to 33 000 $H_2$/Co, under otherwise identical reaction conditions.[80] Losses due to electron back transfer to dehydroascorbic acid are avoided.

For both types of catalysts, glyoxime and polypyridyl-based ones, most reports focus on TONs, TOFs (turnover frequencies), and quantum yields, as a measure of the catalyst's/photocatalytic system's performance. Structure−activity relationships are investigated to systematically improve catalysts.[22,58,59,65,68,79] Mechanistic details are difficult to identify because of the multistep nature of the overall catalytic process. Scheme 1 illustrates the possible routes to $H_2$ formation that are typically considered. The mechanisms differ in the succession of protonation and reduction steps. Starting from $Co^{II}$, which is the resting state of all glyoxime and as well polypyridyl type Co-WRCs during photocatalytic $H_2$ generation, two subsequent reductions result in production of $Co^{I}$ and potentially $Co^{0}$ species. Depending on ligand properties, the second reduction is assigned to a true $Co^{0}$ complex or ligand-based reduction retaining $Co^{I}$.[51,68,70,72,75,81] Both singly and doubly reduced cobalt WRCs can be protonated to their hydride counterparts, $Co^{III}H$ and $Co^{II}H$, respectively. Depending on the kinetics of this step and the follow-up reactions, either an equilibrium is established, or the first protonation becomes the rate limiting step of $H_2$ generation. Cobalt hydrides are believed to be the key intermediates from which $H_2$ can be released, generated in one of two possible ways. Either a second protonation via a hypothetical dihydride/dihydrogen complex leads directly to $H_2$ release, or two cobalt hydrides combine to form hydrogen in a bimolecular process. The former process is a heterolytic pathway (red), while the latter is a homolytic pathway (blue), which refers to the mode of cobalt−hydrogen bond cleavage.

**Scheme 1. Possible $H_2$ Evolution Pathways**

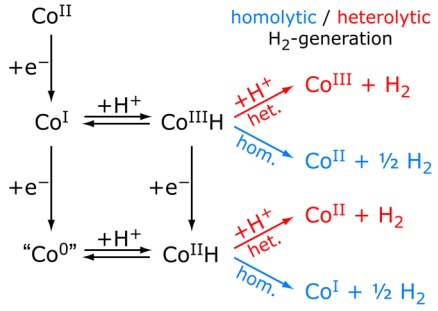


Numerous experimental and theoretical studies have been summarized previously,[38,82] which deal with the mechanism of $H_2$ formation by glyoxime-based Co WRCs. Varying conclusions have been drawn depending on the particular catalyst and reaction conditions. The homolytic and heterolytic mechanisms illustrated in Scheme 1 have been proposed, as well as parallel reactions of both.[22,59,82,83] Recent experimental[61,84] and theoretical[85−87] studies favor the route toward protonation of $Co^{II}H$. In the case of polypyridyl-based catalysts, significantly fewer detailed mechanistic studies are available. Either they focus on selected steps of the mechanism or the conclusions differ from the recent mechanistic proposals for glyoxime-based WRCs.[72,73,79] A particular model system based on the $Co^{I}$(triphos) complex, which allowed monitoring of $H_2$ evolution kinetics by NMR spectroscopy in acetonitrile, was designed by Gray and co-workers.[81] As favored for most glyoxime-based WRCs, the sequence of $Co^{I}$-protonation, reduction to $Co^{II}H$, and a second protonation to release $H_2$, was proposed as the mechanism.

Separate preparation of reduced WRC species would provide a clean starting point for mechanistic investigations but necessitates the use of inert, aprotic solvents. $Co^{I}$ complexes must be stable before addition of an acid, and the time resolution is limited by the mixing of solutes. The latter restriction can be overcome using a photoacid as proton source.[84] The limited choice of solvents is a more severe restriction. Many WRCs do not work or perform only poorly in aqueous solution, indicative that a protic, polar environment is a crucial reaction condition, which may change the key steps of the mechanism or at least affect their kinetics and the position of the associated equilibria.

For time-resolved spectroscopic studies in aqueous solution, only the photocatalytic in situ generation of reduced WRC species is suitable. As a consequence, the overall catalytic system is complicated by the presence of the photosensitizer and sacrificial reductants such as (tertiary) amines[46,88−90] or ascorbate.[46,78,91−93] Reactive radical intermediates formed upon electron donation give rise to rich chemistry and interfere with the desired catalytic process. In photocatalytic hydrogen production, radical species may provide a second electron[56,94−98] or participate in back electron transfers[73,78,91,95,99] depending on their reduction potentials. Hydrogen atom abstraction, addition to double bonds, and fragmentation are further typical elementary follow-up reactions of free radicals.[100−103] Disproportionation and dimerization conclude the chain of possible radical transformations and leave nonradical oxidation products of the sacrificial donors.[94,104−108]

All of these reactions have been investigated in detail for organic radicals and have to be considered in samples containing sacrificial electron donors. These potential side reactions add further complexity to a complete system for photocatalytic hydrogen generation in which many reaction steps from quenching to hydrogen release are covered at once. Altogether, these complications provide an explanation as to why no detailed time-resolved spectroscopic studies are available for photocatalytic systems working in aqueous solution. In the present work, steps toward filling this gap are taken. The combination of laser flash photolysis spectroscopy with the time-resolved detection of $H_2$ by a clark-type hydrogen electrode provides mechanistic insight into proton reduction catalyzed by a polypyridyl-based cobalt WRC. The detailed understanding of the reaction should aid rational improvement of catalysts and identify limitations imposed due to the current need of sacrificial donors.


DOI: 10.1021/ic502591a
Inorg. Chem. 2015, 54, 646−657

## RESULTS AND DISCUSSION

**Photocatalytic System.** The three-component system used throughout this study consists of the photosensitizer (PS) *fac*-[Re(py)(CO)$_3$bipy](OTf) (**1**) (py = pyridine, bipy =2,2′-bipyridine), the water reduction catalyst (WRC) [Co(OH$_2$)(TPY-OH)]$^{2+}$ (**2**) (TPY-OH = 2-bis(2-pyridyl)-(hydroxy)methyl-6-pyridylpyridine), and triethanolamine (TEOA) as sacrificial electron donor (Scheme 2). PS **1** has been used previously in several studies involving proton reduction in aqueous solution, with focus on performance[76,77,80] and mechanistic details of the quenching process.[57,78] TONs as high as 3000 H/Re were reached. The associated $^3$MLCT excited state **1*** has a lifetime of 115 ns in aqueous solution, and is reductively quenched by ascorbate ($k_q$ = 2.6 × 10$^9$ M$^{-1}$ s$^{-1}$, cage escape yield: 0.6) and TEOA ($k_q$ = 5.1 × 10$^7$ M$^{-1}$ s$^{-1}$, cage escape yield: 0.75). Quenching yields the strong one-electron reductant **1**$^-$ with $E_{1/2}$ = −1.54 V versus Fc/Fc$^+$ in DMF (see Supporting Information Figure SI1). Apart from weakly absorbing blue light, **1** lacks any absorption throughout the visible spectrum. While unfavorable for efficient solar light harvesting, **1** is ideal for flash photolysis studies, since visible probe light does not induce photochemistry as in the case of [Ru(bipy)$_3$]$^{2+}$ as PS. In contrast, the reduced PS (**1**$^-$) is intensely blue with broad absorption throughout the whole visible range. The spectrum of **1**$^-$ was obtained by flash photolysis measurements. Absorption maxima are observed at ∼470 and ∼850 nm. The extinction coefficient is 6020 M$^{-1}$ cm$^{-1}$ ± 10% at 500 nm (see Supporting Information SI2 for details.).

**Scheme 2. Depiction of Photosensitizer 1 and Water Reduction Catalyst 2**

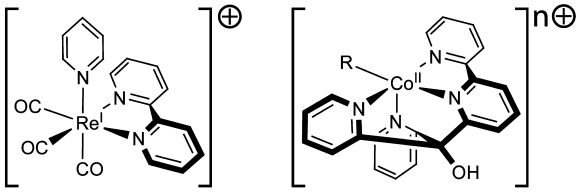


[Re$^{I}$(py)(CO)$_3$bipy]$^+$ (**1**) [Co$^{II}$(R)(TPY-OH)]$^{n+}$
R = Br$^-$, n = 1 (**2a**)
R = OH$_2$, n = 2 (**2**)

WRC **2** was synthesized and used later on for all experiments as its dibromide derivative [CoBr(TPY-OH)]Br (**2a**), the crystal structure of which has been reported previously: A pentacoordinate (TPY-OH)-bromide complex was found along with a bromide counteranion.[76] Compound **2a** was tested before for catalytic performance in combination with ascorbate as the electron donor.[76] TONs as high as 9000 H$_2$/Co were reached at 0.1 μM catalyst concentration. Although it could be shown in the previous study that the catalyst remained unchanged after dissolution in water and during photocatalysis, the determination of the active WRC species present in aqueous solution still required further investigations. With the help of $^{79}$Br NMR spectroscopy,[109] it was possible to quantify the concentration of solvated bromide in an aqueous solution of **2a** and thereby establish that the bromide ligand dissociates quantitatively (see Supporting Information SI3 for details). Bromide is most likely replaced by an aquo ligand, and WRC **2** is formed, which is expected to be the catalytically active complex. Titration of an aqueous solution of **2** excluded the formation of cobalt−hydroxo species within the pH range investigated in this study (pH ≤ 8.75).

The formation of the aquo complex **2** is backed by electronic structure calculations. A geometry optimization based on B97D/Def2-TZVPP electronic structure calculations in water environment revealed a distorted square-pyramidal coordination geometry for [Co(TPY-OH)OH$_2$]$^{2+}$ (**2**) in analogy to the structure observed in case of **2a** (see Supporting Information SI4 for details). The bound Co−O distance is 2.039 Å, which compares well with other aquo complexes where the Co−O distances range between 2.02 and 2.15 Å (mean ±1σ).[110] Attempts to attach a second aquo ligand to generate a hexacoordinate complex led to no binding; the unbound second water drifts into the first solvation shell (Co−O = 2.492 Å).

The UV spectrum of **2** in water shows two intense bands at 250 nm ($\varepsilon$ = 14 500 M$^{-1}$ cm$^{-1}$) and 305 nm ($\varepsilon$ = 12 500 M$^{-1}$ cm$^{-1}$) originating from $\pi$−$\pi^*$ transitions (see Supporting Information SI5). An aqueous solution of **2** is of weakly beige color caused by a shoulder shaped absorption extending from the UV up to ∼650 nm, which appears to be composed of several weak transitions (see Supporting Information SI6). Another weak band is observed in the near-infrared region beyond ∼750 nm. A wB97xD/Def2-TZVPP computed UV−vis spectrum, which shows strong bands at ∼280 nm and at ∼293 nm and only weak bands from 300 to 550 nm followed by a gap and several weak transitions between 750 and 980 nm (see Supporting Information SI4 for the calculated transitions), compares well with these observations.

Compound **2a** is reversibly reduced to a Co$^{I}$ complex in DMF at −1.49 V versus Fc/Fc$^+$, 50 mV positive of the half wave potential of **1**$^-$/**1** (see Supporting Information Figure SI1). A spectrum of the Co$^{I}$ complex was obtained by chemical reduction of **2a** by decamethylcobaltocene in dry DMF (see Supporting Information Figure SI7). It features a broad absorption throughout the whole visible spectral range with a maximum at 638 nm ($\varepsilon$ = 5300 M$^{-1}$ cm$^{-1}$).

While ascorbate is optimal for testing catalytic performance due to the low p$K_a$ of 4.1, it is beneficial to use TEOA for mechanistic studies. If ascorbate is used as electron donor, H$_2$ evolution competes with back electron transfer to ascorbate radicals and reduction of dehydroascorbic acid. These parallel reactions preclude any precise mechanistic studies beyond the electron transfer to the WRC in photocatalytic systems.[73,79,99] The time scale on which H$_2$ is produced is limited roughly by the time after which back electron transfer is completed in absence of WRC. In our case with **1** as PS, this process takes approximately 0.5 ms, and the rate of back electron transfer between **1**$^-$ and ascorbate radicals, $k_{bt}$ = 3.9 × 10$^9$ M$^{-1}$ s$^{-1}$, was measured (see Supporting Information SI8 for details). In the presence of WRC, the strongly reducing Co-species involved in H$_2$ evolution are expected to participate as well in back electron transfers and hence are subject to similar limits. TEOA as donor solves this problem as it is able to provide electrons irreversibly.[96,97] The second benefit of TEOA as sacrificial donor is that it has a p$K_a$ of 7.8. TEOA buffered photocatalytic systems are active in a pH range in which H$_2$ evolution is slower than the typical lifetimes of free radicals, the latter of which are in the range of a few tens to hundreds of microseconds in solution.[101,105,111] The use of TEOA therefore allows a temporal separation between H$_2$ evolution and the generation


DOI: 10.1021/ic502591a
Inorg. Chem. 2015, 54, 646−657

of the active $Co^{I}$–WRC, which is accompanied by side reactions due to radical chemistry.

Laser flash photolysis spectroscopy was used to investigate all processes after reductive quenching of the $^{3}$MLCT excited state **1*** by TEOA, which resulted in $\mathbf{1}^{-}$ as primary reductant. Figure 1a shows difference spectra obtained after laser excitation of a

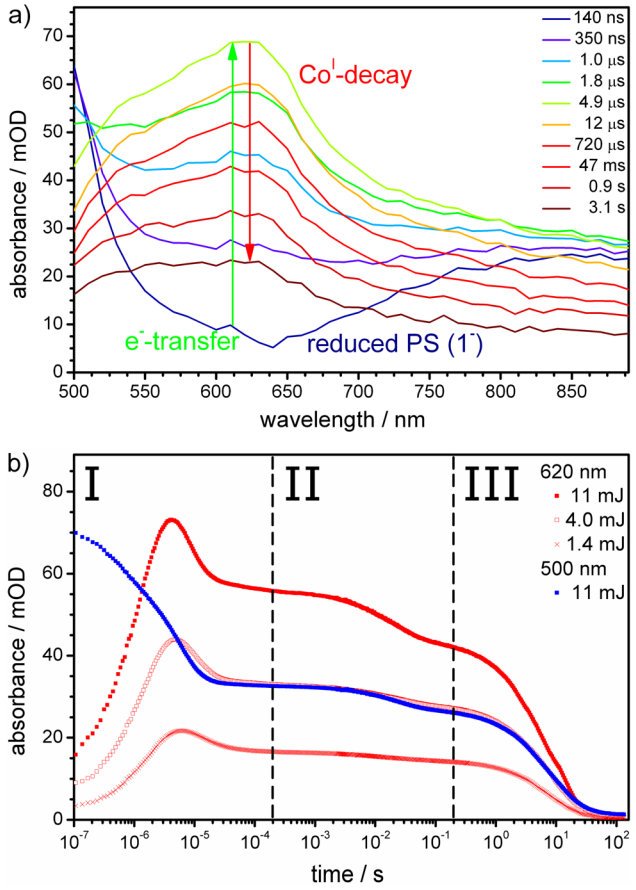


**Figure 1.** Typical spectral and kinetic response in a laser flash photolysis experiment (0.25 mM **1**, 1.0 M TEOA, 0.26 M $HBF_4$, 0.5 mM **2a** in $H_2O$, pH = 8.25). (a) Spectra at different times after 355 nm laser excitation and (b) kinetic traces at 500 and 620 nm for different excitation pulse energies.

TEOA buffered sample containing **1** and **2**. At early times, directly after quenching, absorbance is exclusively caused by the reduced photosensitizer ($\mathbf{1}^{-}$) since no TEOA derived species absorb in the visible spectral range. The spectral signature of $\mathbf{1}^{-}$ disappears on a time scale of a few microseconds, while at the same time a broad absorption with maximum at 620 nm arises. This latter peak is assigned to the $Co^{I}$–WRC generated upon electron transfer from $\mathbf{1}^{-}$ to **2**. A comparison with the spectrum of the reduced WRC in dry DMF, which was synthesized by chemical reduction of **2a** in dry DMF with decamethylcobaltocene, confirms this assignment (see Supporting Information SI7). Both absorption spectra are identically shaped, while the one obtained in aqueous solution is blue-shifted by ∼15 nm due to solvent coordination and different solvent polarities.

Electronic structure theory results for the $Co^{I}$–WRC reveal both a singlet and a slightly more stable triplet state, with an energy difference of only 4.4 kcal/mol. Apparently the coordination geometry, which deviates from the square planar geometry typically taken by $d^{8}$ complexes with singlet ground state, enables a high spin complex with two unpaired electrons. King et al. recently reported a triplet ground state for another, similar $Co^{I}$-polypyridyl complex, which could be synthesized and crystallized.[112] Further calculations provide visible spectra of the $Co^{I}$–WRC (see Supporting Information SI9). The singlet and the triplet state were both considered because of the calculated small energy difference. The former singlet state shows a moderate signal at ∼763 nm ($f$ = 0.06) and strong bands at 404 and 270 nm. In contrast, the triplet state spectral signals are much weaker ($f$ < 0.03), with contributions at 643, 587, 510, 460, and 371 nm. These results can be compared to the protonated state, $Co^{III}H$, which shows strong spectral bands at ∼288 and 235 nm, and between 202 and 209 nm, but no transitions in the visible range (see Supporting Information SI10). Hence, if present in the sample, $Co^{III}H$ is not expected to contribute to the transient absorption spectra in the vis–NIR spectral range.

Eventually, after electron transfer from $\mathbf{1}^{-}$ to **2**, the absorption of $Co^{I}$ decays uniformly without further spectral changes between 500 and 890 nm. Despite the surprising lack of spectral diversity, rich kinetics are observed throughout this decay. Exemplary kinetic traces from the same experiment are shown in Figure 1b. Comparison of the 500 nm trace, where $\mathbf{1}^{-}$ dominates absorption, and the 620 nm trace, which represents $Co^{I}$, illustrates the initial electron transfer. A striking observation is that subsequently the $Co^{I}$-decay occurs in three distinctly separated steps on time scales of a few tens of microseconds, tens of milliseconds, and finally between one second and half a minute. It is therefore straightforward to split the treatment of the overall $Co^{I}$-decay at 200 $\mu$s and 200 ms (dashed vertical lines in Figure 1) and separate reactions, which are related to generation of the reduced WRC (phase I) from further reaction steps ending with the release of $H_2$ (phases II and III).

**Phase I: Electron Transfer and Follow-Up Reactions Related to TEOA Radicals.** In the present TEOA-buffered system the rate of electron transfer between $\mathbf{1}^{-}$ and **2**, $k_{tr}$ = 1.7 × $10^{9}$ $M^{-1}$ $s^{-1}$, was measured. The rate was obtained from laser flash photolysis data by a global fit of the decay of $\mathbf{1}^{-}$ and the rise of the $Co^{I}$ absorption between 500 and 890 nm using the spectra of $\mathbf{1}^{-}$ and $Co^{I}$, shown in Supporting Information SI2 and SI7, as reference. A slightly larger value was determined previously in ascorbate buffer due to the lower viscosity relative to concentrated TEOA solutions.[76] Electron transfer overlaps partially with the subsequent decay of the $Co^{I}$ absorption on a time scale of a few tens of microseconds. This decay could be explained in two ways. Either a protonation equilibrium between $Co^{I}$ and $Co^{III}H$, the latter being spectroscopically close to silent in the visible spectral range, or back reactions due to TEOA-derived radicals could cause the decay of $Co^{I}$. An experiment without **2** as electron acceptor confirms back electron transfer as the reason for the decay step (Figure 2). A three-step decay of the absorption of $\mathbf{1}^{-}$ is observed in this case, while no new absorption bands appear within the visible spectral range. After reductive quenching $\mathbf{1}^{-}$ and TEOA-derived radicals are the only reactive species present in solution, which simplifies the interpretation of the individual decay steps. It is known that $\mathbf{1}^{-}$ is not stable in aqueous solution and ultimately decomposes to the aquo complex *fac*-$[Re(OH_2)(CO)_3bipy]^{+}$ as the final product.[57,113] The last step of the decay of $\mathbf{1}^{-}$ is assigned to this process. Hence, the two faster decay steps occur due to reactions of $\mathbf{1}^{-}$ with TEOA-derived species.


DOI: 10.1021/ic502591a
Inorg. Chem. 2015, 54, 646–657

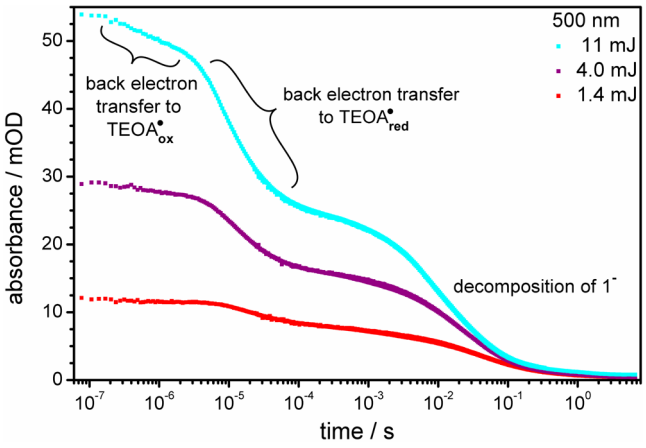


**Figure 2.** Three-step decay of the absorption of $\mathbf{1}^-$ in the absence of WRC **2** as electron acceptor (0.25 mM **1**, 1.0 M TEOA, 0.1 M $HBF_4$ in $H_2O$, pH = 8.75). Three different laser pulse energies were used to generate different starting concentrations of $\mathbf{1}^-$.

Given the above results, it became necessary to consider the follow-up chemistry of TEOA-derived radicals, which has been investigated in several previous studies.[95−97,114,115] According to reaction 1 in Scheme 3, reductive quenching of **1*** by TEOA releases a strongly oxidizing, nitrogen centered radical cation, $R_3N^{\bullet+}$ ($TEOA^{\bullet}_{ox}$), with an oxidation potential of $E(TEOA^{\bullet}_{ox}/TEOA)$ = 0.82 V.[97] This radical is subject to diffusion limited back electron transfer (3) from the strongly reducing PS $\mathbf{1}^-$. The reaction would run to completion within a few hundreds of microseconds if $TEOA^{\bullet}_{ox}$ would not convert to a different, strongly reducing alkyl radical $TEOA^{\bullet}_{red}$. The latter is formed by H atom abstraction from TEOA, which is induced by $TEOA^{\bullet}_{ox}$ according to reaction 5. The rate of this reaction, $k_{abs}$ = 3.3 × $10^6$ $M^{-1}$ $s^{-1}$, has been measured previously by Chan et al.[96] The major product of H atom abstraction is the strongly stabilized[116,117] α-aminoalkyl radical $TEOA^{\bullet}_{red}$,[118,119] but it may be accompanied by smaller amounts of the corresponding α-hydroxyalkyl radical if the H atom is abstracted from the α-hydroxy methylene group of TEOA.[96,97] For a 0.9 M solution of TEOA, the bimolecular rate of H atom abstraction converts to a pseudo-first-order rate with a time constant of 340 ns. The reaction competes with back electron transfer from $\mathbf{1}^-$, which manifests in the first small decay step of $\mathbf{1}^-$ up to ∼1.5 μs shown in Figure 2. H atom abstraction is fast enough that back electron transfer, even at diffusion limited rate, plays only a minor role with relative losses of $\mathbf{1}^-$ below 10% in the case of the largest concentration of $\mathbf{1}^-$. Due to the competition between H atom abstraction (5) with pseudo-first-order kinetics and the second order back electron transfer (3), the significance of the latter is further diminished for smaller concentrations of $\mathbf{1}^-$ and $TEOA^{\bullet}_{ox}$.

**Scheme 3. Reductive Quenching, Electron Transfer, and Follow-Up Reactions Involving TEOA-Related Species (R = $-CH_2CH_2OH$)**[a]

Reductive Quenching

$$1^* + R_3\bar{N} \xrightarrow{k_q} 1^- + R_3\dot{N}^+ \quad (TEOA^{\bullet}_{ox}) \qquad (1)$$

Electron Transfer

$$1^- + Co^{II} \xrightarrow{k_{tr}} 1 + Co^{I} \qquad (2)$$

Back Electron Transfers vs. H-Atom Abstraction

$$1^- + R_3\dot{N}^+ \xrightarrow{k_3} 1 + R_3\bar{N} \qquad (3)$$

$$Co^{I} + R_3\dot{N}^+ \xrightarrow{k_4} Co^{II} + R_3\bar{N} \qquad (4)$$

$$R_2\bar{N}\!\smile\!OH + R_3\dot{N}^+ \xrightarrow{k_{abs}} R_2\bar{N}\!\cdot\!\smile\!OH + R_3NH^+ \quad (TEOA^{\bullet}_{red}) \qquad (5)$$

Back Electron Transfers vs. Radical Deactivation

$$1^- + R_2\bar{N}\!\cdot\!\smile\!OH + H^+ \xrightarrow{k_6} 1 + R_3\bar{N} \qquad (6)$$

$$Co^{I} + R_2\bar{N}\!\cdot\!\smile\!OH + H^+ \xrightarrow{k_7} Co^{II} + R_3\bar{N} \qquad (7)$$

$$2\ R_2\bar{N}\!\cdot\!\smile\!OH \xrightarrow{+H^+} R_2N^+\!\smile\!OH + R_3\bar{N} \qquad (8)$$

$$2\ R_2\bar{N}\!\cdot\!\smile\!OH \longrightarrow R_2\bar{N}\!\smile\!OH + R_3\bar{N} \qquad (9)$$

$$2\ R_2\bar{N}\!\cdot\!\smile\!OH \longrightarrow \text{Dimerization} \qquad (10)$$

[a]Reactions written in black proceed in samples without WRC **2** as electron acceptor while the blue ones additionally contribute to the overall kinetics in the presence of **2**.

The second loss of $\mathbf{1}^-$ takes place on a time scale of a few tens of microseconds and coincides with typical lifetimes of micromolar concentrations of free alkyl radicals in solution.[104,105] Apparently, a second back electron transfer reaction involving $TEOA^{\bullet}_{red}$ is taking place, which is at first sight contrary to the strongly reducing character of the radical. While it is well-known that α-aminoalkyl radicals are strong reductants, rigorous estimations of their reduction potentials are rare due to experimental difficulties associated with their generation and limited lifetime. For α-aminoalkyl radicals derived from tertiary amines, Griller and co-workers have reported oxidation potentials $E$(iminium ion/radical) between −0.9 and −1.1 V versus SCE in acetonitrile.[120] Whitten and co-workers estimate −1 V for the alkyl radical derived from triethylamine in water.[94] The most detailed studies related to the role of TEOA-derived radicals in photocatalysis use methyl viologen with $E°(MV^{2+}/MV^{+})$ = −0.45 V versus SHE[121] as electron acceptor.[96,97] In aqueous solution, $TEOA^{\bullet}_{red}$ is sufficiently reducing to transfer an electron to $MV^{2+}$. We observed quantitative transfer of a second electron as well for $MV^{2+}$ as acceptor, and made use of this behavior for quantification of the extinction coefficient of $\mathbf{1}^-$ (see Supporting Information SI2). In absence of $MV^{2+}$, i.e., in a sample containing only **1** and the TEOA/$HTEOA^+$ quencher/buffer, **1** is the only potential electron acceptor. As shown in Figure 2, apparently no transfer of a second electron takes place in this case due to the low reduction potential $E(\mathbf{1}/\mathbf{1}^-)$. Instead, back electron transfer (6) is observed on the time scale of a few tens of microseconds, and appears to compete with possible disproportionation and dimerization radical deactivations as in reactions 8, 9, and 10 which leave much less reactive nonradical oxidation products of TEOA. Glycolaldehyde and diethanolamine were found as final products indicating the dominant formation of the iminium ion in reaction 8, which slowly hydrolyzes in aqueous solution.[118,119] As a consequence of the competition between radical deactivation and back electron transfer, a fraction of $\mathbf{1}^-$ is preserved. It is noteworthy that, for very low transient concentrations of $\mathbf{1}^-$, back electron transfer becomes much slower due to a quadratic dependence of the observed rate on concentration. In a previous step-scan FT-IR experiment, the concentration of $\mathbf{1}^-$ remained close to constant for 200 μs.[78]

In the presence of WRC **2**, the role of back electron transfer reactions stays the same (Figure 1). As shown in reaction 2,


DOI: 10.1021/ic502591a
Inorg. Chem. 2015, 54, 646−657

electron transfer from $\mathbf{1}^-$ to $Co^{II}$ generates $Co^{I}$, which is only a slightly less strong reductant than is $\mathbf{1}^-$ ($\Delta E$ = 0.05 V in DMF) and participates in the same back electron transfers to TEOA-derived radicals as observed for $\mathbf{1}^-$. While the fast electron losses from $\mathbf{1}^-$ and $Co^{I}$ to $TEOA^{\bullet}_{ox}$ (reactions 3 and 4) are hidden by the electron transfer (2), which takes place on the same time scale, the slower back electron transfer from $Co^{I}$ to $TEOA^{\bullet}_{red}$ (reaction 7) is clearly visible. This process is completed after roughly 50 $\mu$s when TEOA-derived radical species have reacted completely.

**Phase II: Intermediate Decay of $Co^{I}$.** The second part of the $Co^{I}$ kinetics shown in Figure 1 involves the intermediate decay step of the $Co^{I}$ absorbance between 2 and 200 ms. Before this reaction sets in, $Co^{I}$, which remained after back electron transfer, and the nonradical oxidation products of TEOA (mainly the iminium salt formed in reaction 8), are present in solution. pH dependent measurements with different concentrations of TEOA in addition to a more acidic sample with ascorbate yield identical $Co^{I}$ spectra (see Supporting Information SI11), which confirm the presence of the same $Co^{I}$ species in all samples; TEOA as a potential ligand does not influence $Co^{I}$ through coordination.

Figure 3a shows pH-dependent measurements of the $Co^{I}$ decay starting from 200 $\mu$s, which proceeds in two distinct steps. The rate of the second and final $Co^{I}$ decay step depends on the concentration of protons, $[H^+]$, while a visual comparison of the kinetic traces with respect to the intermediate decay step between 2 and 200 ms is not directly possible due to the different starting concentrations of $Co^{I}$. A second set of pH-dependent kinetic traces, which enables a direct comparison of the intermediate $Co^{I}$ decay, is shown in Figure 3b. Equal starting concentrations of $Co^{I}$ were achieved in this case by slightly varying excitation energies for each sample in order to compensate for decreasing quenching yields and increasing losses due to back electron transfer at lower pH. The comparison reveals that the kinetics and magnitude of the intermediate decay step are not influenced by the pH of the sample. Hence, no protonation is involved in the underlying reaction.

The most striking property of the intermediate decay step of the $Co^{I}$ absorption between 2 and 200 ms is revealed by looking at its dependence on the concentration of $Co^{I}$ (Figure 3c). If the step size was proportional to the concentration of $Co^{I}$, no difference would be observed between the normalized kinetic traces. Instead, the relative size of the intermediate decay step increases with higher concentrations of $Co^{I}$. As elaborated on below, the step size is proportional to the square of the total $Co^{I}$ concentration. The quadratic dependence on the concentration of $Co^{I}$ corresponds either to an equilibrium in which two $Co^{I}$ are involved or an equilibrium reaction of one $Co^{I}$ with another species whose initial concentration is similar to and proportional to the initial concentration of $Co^{I}$.

A straightforward explanation that fulfills that condition would be an equilibrium in which two $Co^{I}$ units dimerize. A process of that kind has the appealing property that it could be a productive step of the overall catalytic mechanism. A potential dimerization combines the two electrons needed for $H_2$ generation in one molecule and could even give rise to a truly bimolecular mechanism of $H_2$ release. However, up to now none of the respective intermediates have been observed. Mandal et al. recently designed a suitable binuclear Co-WRC, which provides two electrons in one molecule and could promote homolytic $H_2$ formation due to the proximity of the

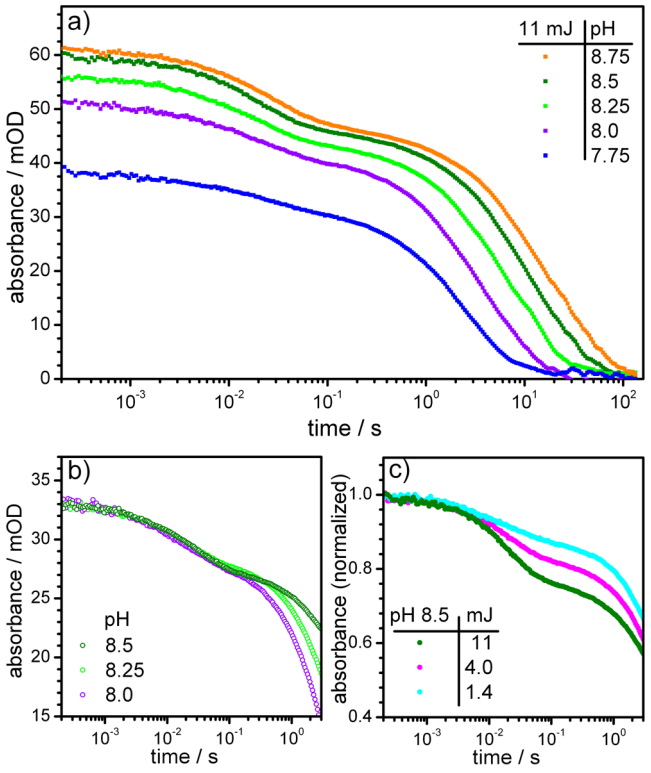


**Figure 3.** Phase II of the $Co^{I}$ decay: (a) As a function of pH (0.25 mM **1**, 0.5 mM **2a**, 1.0 M TEOA, and 0.10/0.17/0.26/0.39/0.53 M $HBF_4$ in $H_2O$) monitored at 620 nm. Different starting concentrations of $Co^{I}$ for identical excitation energies are caused by the decreasing concentration of TEOA within the TEOA/$HTEOA^+$ buffer system at lower pH values. A smaller fraction of **1*** is reductively quenched while the fraction of back electron transfer is increased at the same time (see Phase I section). (b) Same type of measurement as in part a with the excitation energies slightly adjusted around 4 mJ for each pH in order to generate identical starting concentrations of $Co^{I}$. (c) Normalized kinetic traces of the intermediate $Co^{I}$ decay step measured at different laser pulse energies, which result in different concentrations of $Co^{I}$.

cobalt atoms. No interaction between the cobalt centers was found, and instead the protonation of $Co^{III}H$ was proposed as mechanism of $H_2$ release.[72]

Three options for a dimer were envisioned. The two first ones are dinuclear complexes in which the two TPY-OH ligands link the $Co^{I}$ centers via a pyridine site (see Supporting Information SI12 for details). In these structures, one finds slightly distorted square planar coordination geometries for the two $d^8$-$Co^{I}$ metal centers, which is expected to be favored over the distorted geometry enforced by the ligand in the monomeric complexes **2** and **2a**. The third option involves a direct Co−Co interaction. Weak $d^8$−$d^8$ interactions are known for various dimers and even chains of square planar $d^8$ complexes with singlet ground state as $Pt^{II}$, $Pd^{II}$, $Rh^{I}$, and $Ir^{I}$.[122−132] A triplet ground state of $\mathbf{2}^-$ could instead give rise to stronger metal−metal interactions involving the unpaired electrons. The calculated structure of a Co−Co dimer is shown in Supporting Information SI13. Electronic structure calculations using a continuum-cluster environment for the proper treatment of coordinated water molecules suggest that all of the three dimers are energetically feasible. Nevertheless, spectral calculations predict significant absorption throughout the visible spectral range in all cases (see Supporting


DOI: 10.1021/ic502591a
Inorg. Chem. 2015, 54, 646−657

Information SI12 and SI13). Contrary to the thermodynamic stability, neither of the dimers seems to be suited to explain the intermediate decay step of $Co^{I}$ since no new absorption bands of the reaction product(s) are observed experimentally.

Besides a dimerization equilibrium a reaction of $Co^{I}$ with the iminium ion formed in reaction 8 provides a viable explanation of the intermediate decay step. The latter compound is the only component in the sample with a concentration similar, and at the same time proportional, to that of $Co^{I}$, which is required for the description of the observed step in the experimental data. An equilibrium reaction between $Co^{I}$ and the iminium ion results in the correct dependence of the step size on the concentration of $Co^{I}$. $Co^{I}$ complexes are known to be excellent cobalt nucleophiles, particularly vitamin $B_{12}$ derivatives, which are often termed as "super nucleophiles" with Pearson nucleophilicity indexes exceeding that of iodide and other effective nucleophiles by far.[133] The reactivity of corrin-based and other $Co^{I}$ complexes in nucleophilic substitutions and additions has been studied intensely, particularly due to the biologic relevance of vitamin $B_{12}$.[133−137] In the present case it is reasonable to assume that $Co^{I}$ could add to the iminium ion as a suitable electrophile, as schematically represented by eq 11.

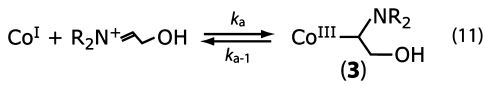

(11)

The reaction is expected to be reversible in analogy to aminal/hemiaminal chemistry, where additions of nucleophiles are generally equilibrium reactions and substrates are prone to hydrolysis. A closely related example of formation of an $\alpha$-aminoalkyl cobalt complex was reported by Schrauzer and co-workers.[138]

Adduct **3** is a $Co^{III}$ complex, which would readily explain the lack of absorption in the visible spectral range, as is observed experimentally. To confirm this hypothesis, B97D/Def2-TZVPP electronic structure calculations in water environment were done, which predict an octahedral complex for the proposed adduct **3**, with both the $\alpha$-aminoalkyl ligand as well as a water ligand as schematically shown in Figure 4. The structural data are given in Supporting Information SI14.

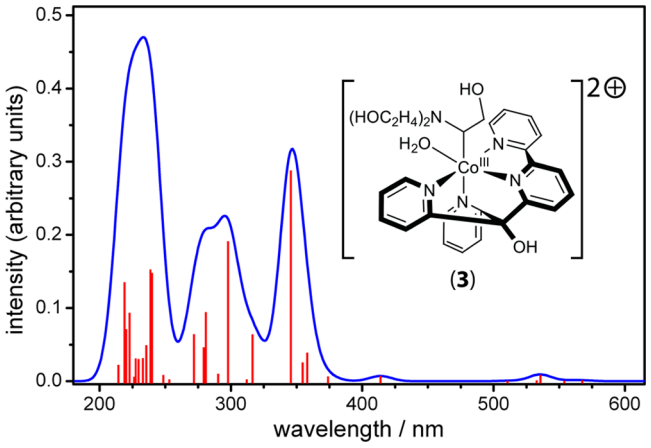


**Figure 4.** Schematic drawing of the structure of adduct **3**, together with the associated wB97xD/Def2-TZVPP computed spectrum. The 30 transitions with lowest energies were included in the simulation of the spectrum and convoluted with a Gaussian of 20 nm fwhm for a visual representation.

Compound **3** is stabilized by 15 kcal/mol relative to the reactants $Co^{I}$(singlet) and the iminium ion according to reaction 11. The calculated spectrum contains intense bands at 345 nm ($f$ = 0.29), 298 nm ($f$ = 0.19), and 239 nm ($f$ = 0.15), in addition to several weaker bands, which are exclusively appearing in the UV. Two very weak bands are predicted in the visible range at 414 and 536 nm, which might not be detectable at the very low concentrations of the adduct produced in the experiments. Unlike in the cases of the three potential dimers, the results of the quantum chemical calculations are consistent with the experiments. Hence, the reversible formation of **3** is preferred over the formation of a dimer as explanation of the intermediate decay step of $Co^{I}$.

**Phase III: Proton Reduction and $H_2$ Release.** Up to and including the intermediate decay step of $Co^{I}$, no indication for protonation was found, and the final decay of $Co^{I}$ is the first process with rate proportional to $[H^+]$ as shown in Figure 3a. This could be caused either by a slow, quantitative protonation of $Co^{I}$, or by a follow-up reaction involving $Co^{III}H$. $Co^{I}$ can exist in equilibrium with a small fraction of $Co^{III}H$, the existence of which does not manifest before the final decay. Due to the protonation equilibrium, the rate of the latter reaction would be proportional to $[H^+]$ as well. In order to gain more detailed insight, it is necessary to correlate the final decay of $Co^{I}$ with the release of $H_2$. Since the decay of $Co^{I}$ happens on the time scale of seconds to minutes, the time resolved detection of $H_2$ along with precise quantification becomes possible. A clark-type hydrogen electrode with a response time of 0.9 s was used for this purpose (see Supporting Information SI15). The pH-dependent measurements shown in Figure 5

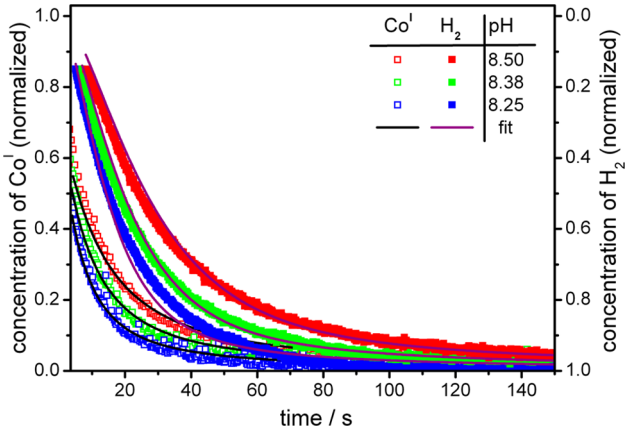


**Figure 5.** Decay of $Co^{I}$ measured simultaneously with the delayed production of $H_2$ (0.25 mM **1**, 0.2 mM **2a**, 1.0 M TEOA and 0.10/0.21/0.26 M $HBF_4$ in $H_2O$). The kinetic traces are shown together with the fits as obtained with the model elaborated below. The $H_2$ transients were normalized to the final concentration of $H_2$ as measured by the calibrated clark-type hydrogen electrode. The kinetic traces representing the $Co^{I}$ decay were normalized to the corresponding initial concentrations of $Co^{I}$, which yield the respective amount of $H_2$ after completion of catalysis.

revealed $H_2$ evolution, which is slightly delayed relative to the $Co^{I}$ decay. Nevertheless, the rate is proportional to $[H^+]$, which indicates that a second protonation is directly involved in the release of $H_2$. At the same time, the delay requires the accumulation of a reaction intermediate on the way from $Co^{I}$ to $H_2$ release. Together these findings can only be explained by an overall mechanism with two separate protonation steps and


DOI: 10.1021/ic502591a
Inorg. Chem. 2015, 54, 646−657

consequent transient accumulation of a cobalt hydride as intermediate. Both homolytic mechanisms depicted in Scheme 1 do not fulfill this condition, since $H_2$ release from two molecules of $Co^{III}H/Co^{II}H$ would not be pH-dependent in case of transient accumulation of the hydride.

**Evaluation of $H_2$ Evolution Mechanisms.** Two options from the general mechanistic scheme remain for consideration: either there could be protonation of $Co^{III}H$ directly yielding $H_2$ in analogy to the mechanism proposed by Fukuzumi and co-workers,[72] or $Co^{III}H$ could be reduced by $Co^{I}$ to $Co^{II}H$ first, as found by Gray and co-workers.[81] The former pathway is only in agreement with a linear dependence of the $Co^{I}$ decay on $[H^+]$ if the first protonation is rate limiting and "irreversible"; i.e., the protonation equilibrium is never established. Otherwise, a quadratic dependence of the $Co^{I}$ decay rate on $[H^+]$ is expected since the rate of the second protonation would be connected to the protonation equilibrium $Co^{I}/Co^{III}H$. Both pathways were compared by globally fitting the corresponding systems of rate equations to the spectroscopic and $H_2$ data at different pH (see Supporting Information SI16 for details). The intermediate decay step was included as reversible side reaction according to the formation of **3**, the adduct of $Co^{I}$, and the iminium ion. Only the mechanism including the intermediate reduction of $Co^{III}H$ to $Co^{II}H$, as summarized in Scheme 4, is able to reproduce the complete data set.

**Scheme 4. Mechanism of $H_2$ Generation Found for 2 in Aqueous Solution**

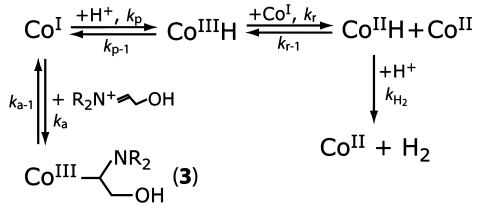


Figures 5 and 6 show exemplary kinetic traces from laser flash photolysis and $H_2$ measurements together with the global fit (solid lines). The model is able to reproduce the intermediate decay step of $Co^{I}$, including its concentration dependence and pH independence, as well as the linear dependence of the $Co^{I}$ decay on $[H^+]$. The final decay of $Co^{I}$ follows neither purely exponential first order nor second order kinetics but is a mixture between the two cases indicating that there is not a single rate-determining step. The protonation of $Co^{I}$ as well as the reduction of $Co^{III}H$ contribute to the observed decay kinetics of $Co^{I}$. For comparison, the best fit obtained with the model involving direct protonation does not reproduce the data since it is limited to exponential $Co^{I}$ decay kinetics (see Supporting Information SI17).

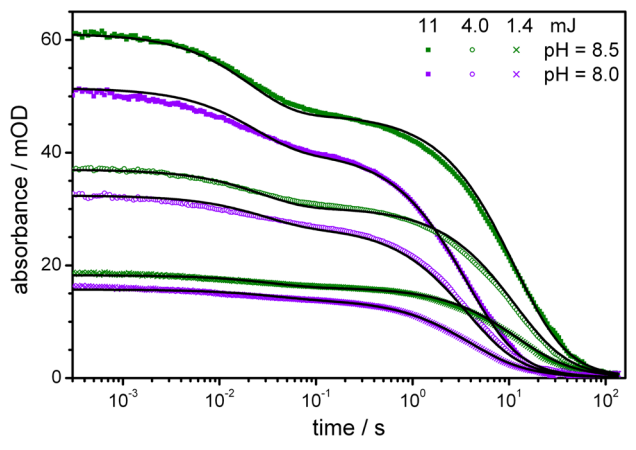


**Figure 6.** Fit shown for exemplary kinetic traces of the $Co^{I}$ decay (0.25 mM **1**, 0.5 mM **2a**, 1.0 M TEOA, and 0.17/0.39 M $HBF_4$ in $H_2O$). The global fit included all kinetic traces shown in Figure 3 with three different excitation energies for each pH.

Figure 7 shows concentration profiles for one experiment as obtained from the global fit according to the mechanism shown in Scheme 4. The adduct formation equilibrium is established on the time scale of few tens of milliseconds with $k_a = 5 \times 10^5$ $M^{-1}$ $s^{-1}$ and $k_{a-1} = 2 \times 10^1$ $s^{-1}$ as forward and backward rates and the corresponding equilibrium constant $K = 2.5 \times 10^4$ $M^{-1}$. $Co^{I}$ is protonated with the rate $k_p = 1.7 \times 10^7$ $M^{-1}$ $s^{-1}$. $Co^{III}H$ is not accumulated due to the follow-up reduction by $Co^{I}$ to $Co^{II}H$. The latter reaction is found to be fast and irreversible with a $k_r$ between $10^8$ and $10^{10}$ $M^{-1}$ $s^{-1}$. The rate of the reverse reaction is minimized during the fitting procedure, which results in negligibly small values for $k_{r-1}$. For the rates of the reduction of $Co^{III}H$, $k_r$, and the deprotonation of $Co^{III}H$, $k_{p-1}$ = $10^3$–$10^5$ $s^{-1}$, only crude approximations are obtained since the two reactions are linked. They compete with each other; i.e., the effect of a slower deprotonation rate is compensated by a slower reduction without significantly changing the fit. $Co^{II}H$ is accumulated transiently as required by the delay between the $Co^{I}$ decay and $H_2$ release. A rate of $k_{H2} = 2.2 \times 10^7$ $M^{-1}$ $s^{-1}$ is obtained for the protonation of $Co^{II}H$.

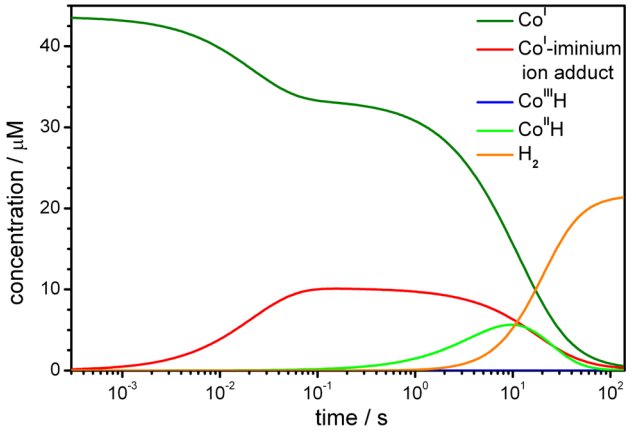


**Figure 7.** Concentration profiles as obtained from the fit of the $Co^{I}$ protonation, $Co^{III}H$ reduction, and $Co^{II}H$ protonation model with the $Co^{I}$–iminium ion adduct as reversible side reaction (pH = 8.5, 11 mJ excitation pulse energy, see Figure 6 for the corresponding 620 nm transient).

## SUMMARY AND CONCLUSION

Comprehensive spectroscopic studies in combination with the time-resolved quantification of $H_2$ production revealed the mechanism of $H_2$ release. Computational analyses of spectra and thermodynamic properties of intermediates and products of side reactions were used to assign individual steps of the mechanism to the spectroscopic observations. The detection and quantification of $H_2$ confirmed that the catalyst is working properly in a freshly prepared, well-defined sample. This confirmation is mandatory since, in experiments used for testing the performance of catalysts, the sample is typically



DOI: 10.1021/ic502591a
Inorg. Chem. 2015, 54, 646–657

irradiated continuously and in some cases an induction period is observed before $H_2$ is produced.

In the investigated system, electrons for $H_2$ production are provided by TEOA, which reductively quenches the $^3$MLCT state of the PS **1**. The electrons are collected by the WRC **2**, which serves as catalyst and electron reservoir in its reduced form $\mathbf{2}^-$ ($Co^I$) at moderately basic pH. $H_2$ is produced after protonation of $Co^I$ to $Co^{III}H$, reduction of the latter by $Co^I$ to $Co^{II}H$, and finally protonation of $Co^{II}H$. The rate of the transformation of $Co^I$ to $Co^{II}H$ is determined by both intermediate reaction steps, the protonation and the comproportionation, depending on the total concentration of $Co^I$.

The mechanism agrees with the more recent findings for glyoxime-based WRCs[61,84−87] and the model system based on the $Co^I$(triphos) complex.[81] For polypyridyl-based WRCs, fewer results are available that would enable comparison. Mandal et al. investigated the role of bimolecular $H_2$ evolution pathways with the aid of a binuclear $Co^ICo^I$ complex in acetonitrile.[72] No interaction of the two Co centers was observed, and the direct protonation of $Co^{III}H$ yielding $H_2$ and $Co^{III}$, which is reduced immediately in the presence of additional $Co^I$, was proposed. Apparently the mechanism of $H_2$ production is, as stated for glyoxime-based WRCs,[38,52,83,87] sensitive to the reaction conditions. Singh et al. characterized a cobalt−polypyridyl complex electrochemically in aqueous solution,[73] and were able to exclude bimolecular $H_2$ formation on the time scale of cyclic voltammetry. They found evidence for formation of $Co^{III}H$ and proton coupled electron transfer during electrochemical reoxidation of the hydride. Time resolved spectroscopic studies beyond the electron transfer between the reduced PS and the WRC were prevented by back electron transfer to ascorbate radicals, which dominated the decay of the reduced WRC in flash photolysis experiments. Hence, their findings do not contradict the results presented within this work, but a strict comparison is not possible without further investigations.

A second focus was put on side reactions involving TEOA-derived species. This sacrificial electron donor is widely treated as a necessary but mostly innocent electron donor. The role of electron back transfers was assessed and compared to the reports in the literature. Not only was the well-known back electron transfer to the nitrogen-centered radical cation observed[95−97] but also the subsequently formed $\alpha$-amino radical is involved in back electron transfers if sufficiently strong reductants as $\mathbf{1}^-$ and $\mathbf{2}^-$ are present. Apart from the reactions of the radical species, an additional side reaction involving the nonradical oxidation product of TEOA, an iminium ion, is proposed: $Co^I$ adds reversibly to the electrophilic iminium group forming an adduct with a cobalt−carbon bond. Other potential explanations for the observed side reaction could be excluded with the help of quantum chemical calculations. In conclusion, TEOA is less of an irreversible, innocent electron donor as often assumed. The participation of TEOA derived species in side reactions accompanying the whole process of $H_2$ formation complicates mechanistic investigations severely. Nevertheless, a detailed understanding will help the search for better catalysts, and enable one to separate limitations due to the actual catalyst from problems associated with the sacrificial donor, which is currently necessary but will be ultimately replaced by water oxidation in a complete water splitting system.

## EXPERIMENTAL SECTION

**Chemicals.** Grade 1 $H_2O$ according to ISO 3696 was provided by a Milli-Q purification system. Analytical grade TEOA and aqueous $HBF_4$ were purchased from Sigma-Aldrich. Spectroscopic grade DMF was purchased from Acros, and electrochemical grade [TBA][$PF_6$] from Fluka. All chemicals were used without further purification. The syntheses of **1** and **2a** have been described previously.[57,76]

**Sample Preparation.** Stock solutions of **1** (1 mM), **2a** (5 mM), and TEOA (2.5 M) were prepared with degassed $H_2O$ and stored under Ar atmosphere. They were used in the general procedure of sample preparation: Appropriate amounts of the TEOA stock solution and 8 M $HBF_4$ were mixed and degassed by bubbling Ar through the solution for 30 min before the stock solutions of **1** and **2a** were added. The sample was filled to the desired volume with degassed $H_2O$ and transferred to an Ar filled cuvette. The cuvette was sealed after another 15 min of bubbling Ar through the sample. All samples were prepared directly before the measurements.

**Laser Flash Photolysis.** was used to measure absorbance changes after laser pulse excitation (Nd:YAG, 355 nm, 6 ns pulse duration) from 30 ns to 140 s and between 500 and 890 nm. A two monochromator setup with single wavelength detection was chosen to minimize the sample's exposure to probe light and to remove most of the phosphorescence emitted by the photosensitizer. A halogen bulb (640−890 nm) and a white light LED (500−640 nm), which provide very stable output power, were used as light sources. The probe light was detected with an amplified silicon photodiode (Hamamatsu S3883, 320−1000 nm spectral response range, 300 MHz bandwidth), and the dc signal was digitized with a 125 MHz bandwidth (200 MS/s, 16 bit resolution) transient recorder. The sample was stored in a sealed, 2 mm quartz cuvette and stirred between laser shots. A small reservoir was introduced directly above the cuvette, to allow sufficiently large sample volumes, so that the whole sample is statistically excited only up to three times throughout a complete measurement. The volume excited by the laser pulse was four times larger than the probed volume to allow measurements up to 140 s before diffusion takes any effect. The loss of absorbance due to sample diffusion was excluded by measuring the persistence of $MV^+$ after 355 nm excitation (sample: 0.25 mM **1**, 5 mM methylviologen hexafluorophosphonate, 1.0 M TEOA, and 0.1 M $HBF_4$ in $H_2O$). For each single wavelength kinetic trace two acquisitions with different sampling rates were stitched in order to cover the complete time range from nanoseconds to minutes. Between two and five acquisitions were averaged each time.

**$H_2$ Clark-Type Electrode Measurements.** A $H_2$ sensitive clark-type electrode (500 $\mu$m tip diameter, selected for a fast response time), purchased from Unisense A/S, was used for the time-resolved quantification of $H_2$. It was calibrated on a daily basis with the help of an aqueous solution of $H_2$ with known concentration. The calibration solution was prepared by bubbling diluted $H_2$ (0.5% in argon) through $H_2O$. Using Henry's law and taking into account the local ambient pressure, the concentration of $H_2$ was calculated from $H_2$ solubility data.[139] The electrode was immersed in the sample, which was contained in a two-neck, 10 mm quartz cuvette. Simultaneously with $H_2$ detection the absorbance of $Co^I$ was monitored with a fiber coupled spectrometer (Ocean Optics USB-4000). Probe light was provided by a fiber coupled halogen light source (Ocean Optics DH-2000-BAL) and collimated before passing through the sample. The cuvette was surrounded by four high power 370 nm LEDs, which ensure close to uniform irradiation of the whole sample. To even out minimal initial inhomogeneities of the $Co^I$ concentration, the sample was stirred throughout the whole measurement with a magnetic stirring bar. Irradiation times between 5 and 50 ms were used to generate varying starting concentrations of $Co^I$.

Electrochemical measurements were carried out in DMF containing 0.1 M [TBA][$PF_6$] as conducting electrolyte. A Metrohm 797VA Computrace electrochemical analyzer was used with a standard three electrode setup of glassy carbon working (i.d. = 2 mm) and Pt auxiliary electrodes and an Ag/AgCl reference electrode. All potentials are given versus $Fc/Fc^+$ unless otherwise noted. Differential pulse voltammo-


DOI: 10.1021/ic502591a
Inorg. Chem. 2015, 54, 646−657

grams were recorded with a voltage step of 6 mV, voltage step time of 0.4 s, a pulse amplitude of 50 mV, and a pulse time of 40 ms, giving a sweep rate of 15 mV/s.

**Computational Methods.** The structural and energetic analyses of the molecular systems described in this study were carried out with the B97-D dispersion enabled density functional method,[140,141] using an ultrafine grid, together with the Def2-TZVPP basis set.[142] Full geometry optimizations were performed and uniquely characterized via second derivatives (Hessian) analysis to establish stationary points and effects of zero point and thermal corrections. Effects of solvent were included using a cluster-continuum solvation model, where the continuum model is based the original COSMO theory of Klamt modified for *ab initio* theory,[143,144] with a dielectric for water. Complexation energies for dimer formation were determined using a bond separation reaction, including an explicit-implicit model of solvation, in accord with [2*Co($x$ = I, II, $y$ = S, T)monomer + ($n$ − 4)watercluster → ($n$)watercluster + dimer complex ($x$ = I, II, $y$ = S, T)]. Optimal explicit water contributions were determined self-consistently on the basis of bond separation reactions for the complexation process for a series of "$n$" in the above equation. Optimal solvent clusters were determined to be ($n$ − 4) = 12 and $n$ = 16, in the complexation reactions, across all combinations of cobalt oxidation state and electronic structure state (singlet, triplet, quartet). Determination of excited states and associated spectra were determined at wB97xD[145]/Def2-TZVPP//B97-D/Def2-TZVPP level of theory. For a visual representation the calculated line spectra were convoluted with a Gaussian.

## ■ ASSOCIATED CONTENT

### Supporting Information

Additional figures and details. This material is available free of charge via the Internet at http://pubs.acs.org.

## ■ AUTHOR INFORMATION


### Corresponding Author

*E-mail: peter.hamm@chem.uzh.ch.


### Notes

The authors declare no competing financial interest.

## ■ ACKNOWLEDGMENTS

We acknowledge the Swiss National Science Foundation (Grant CRSII2_136205/1) and the University of Zurich (URPP LightChEC) for financial support.

## ■ REFERENCES


(1) Lewis, N. S.; Nocera, D. G. *Proc. Natl. Acad. Sci. U.S.A.* **2006**, *103*, 15729−15735.
(2) Cook, T. R.; Dogutan, D. K.; Reece, S. Y.; Surendranath, Y.; Teets, T. S.; Nocera, D. G. *Chem. Rev.* **2010**, *110*, 6474−6502.
(3) Turner, J. A. *Science* **1999**, *285*, 687−689.
(4) *Solar Hydrogen Generation*; Rajeshwar, K., McConnell, R. D., Licht, S., Eds.; Springer: New York, 2008.
(5) Bard, A. J.; Fox, M. A. *Acc. Chem. Res.* **1995**, *28*, 141−145.
(6) Steinfeld, A. *Sol. Energy* **2005**, *78*, 603−615.
(7) Abanades, S.; Charvin, P.; Flamant, G.; Neveu, P. *Energy* **2006**, *31*, 2805−2822.
(8) Funk, J. E. *Int. J. Hydrogen Energy* **2001**, *26*, 185−190.
(9) Kodama, T.; Gokon, N. *Chem. Rev.* **2007**, *107*, 4048−4077.
(10) Eroglu, E.; Melis, A. *Bioresour. Technol.* **2011**, *102*, 8403−8413.
(11) McKinlay, J. B.; Harwood, C. S. *Curr. Opin. Biotechnol.* **2010**, *21*, 244−251.
(12) Melis, A.; Happe, T. *Plant Physiol.* **2001**, *127*, 740−748.
(13) Krishna, R. H. *Eur. J. Biotechnol. Biosci.* **2013**, *1*, 84−93.
(14) Grimes, C. A.; Varghese, O. K.; Ranjan, S. *Light, Water, Hydrogen: The Solar Generation of Hydrogen by Water Photoelectrolysis*; Springer: New York, 2007.
(15) Fujishima, A.; Honda, K. *Nature* **1972**, *238*, 37−38.
(16) Reece, S. Y.; Hamel, J. A.; Sung, K.; Jarvi, T. D.; Esswein, A. J.; Pijpers, J. J. H.; Nocera, D. G. *Science* **2011**, *334*, 645−648.
(17) Boettcher, S. W.; Warren, E. L.; Putnam, M. C.; Santori, E. A.; Turner-Evans, D.; Kelzenberg, M. D.; Walter, M. G.; McKone, J. R.; Brunschwig, B. S.; Atwater, H. A.; Lewis, N. S. *J. Am. Chem. Soc.* **2011**, *133*, 1216−1219.
(18) Kudo, A.; Miseki, Y. *Chem. Soc. Rev.* **2009**, *38*, 253−278.
(19) Grätzel, M. *Nature* **2001**, *414*, 338−344.
(20) Walter, M. G.; Warren, E. L.; McKone, J. R.; Boettcher, S. W.; Mi, Q.; Santori, E. A.; Lewis, N. S. *Chem. Rev.* **2010**, *110*, 6446−6473.
(21) Andreiadis, E. S.; Chavarot-Kerlidou, M.; Fontecave, M.; Artero, V. *Photochem. Photobiol.* **2011**, *87*, 946−964.
(22) Jacques, P.-A.; Artero, V.; Pécaut, J.; Fontecave, M. *Proc. Natl. Acad. Sci. U.S.A.* **2009**, *106*, 20627−20632.
(23) Barber, J.; Tran, P. D. *J. R. Soc., Interface* **2013**, *10*, 20120984.
(24) Wang, M.; Chen, L.; Sun, L. *Energy Environ. Sci.* **2012**, *5*, 6763−6778.
(25) Tran, P. D.; Artero, V.; Fontecave, M. *Energy Environ. Sci.* **2010**, *3*, 727−747.
(26) Kalyanasundaram, K.; Grätzel, M. *Curr. Opin. Biotechnol.* **2010**, *21*, 298−310.
(27) Chen, X.; Shen, S.; Guo, L.; Mao, S. S. *Chem. Rev.* **2010**, *110*, 6503−6570.
(28) Abdi, F. F.; Han, L.; Smets, A. H. M.; Zeman, M.; Dam, B.; van de Krol, R. *Nat. Commun.* **2013**, *4*, 2195.
(29) Carmo, M.; Fritz, D. L.; Mergel, J.; Stolten, D. *Int. J. Hydrogen Energy* **2013**, *38*, 4901−4934.
(30) Ezaki, H.; Morinaga, M.; Watanabe, S. *Electrochim. Acta* **1993**, *38*, 557−564.
(31) Conway, B. E.; Tilak, B. V. *Electrochim. Acta* **2002**, *47*, 3571−3594.
(32) McKone, J. R.; Lewis, N. S.; Gray, H. B. *Chem. Mater.* **2014**, *26*, 407−414.
(33) Cobo, S.; Heidkamp, J.; Jacques, P.-A.; Fize, J.; Fourmond, V.; Guetaz, L.; Jousselme, B.; Ivanova, V.; Dau, H.; Palacin, S.; Fontecave, M.; Artero, V. *Nat. Mater.* **2012**, *11*, 802−807.
(34) DuBois, D. L. *Inorg. Chem.* **2014**, *53*, 3935−3960.
(35) Wiese, S.; Kilgore, U. J.; DuBois, D. L.; Bullock, R. M. *ACS Catal.* **2012**, *2*, 720−727.
(36) Helm, M. L.; Stewart, M. P.; Bullock, R. M.; DuBois, M. R.; DuBois, D. L. *Science* **2011**, *333*, 863−866.
(37) Eckenhoff, W. T.; Eisenberg, R. *Dalton Trans.* **2012**, *41*, 13004−13021.
(38) Artero, V.; Chavarot-Kerlidou, M.; Fontecave, M. *Angew. Chem., Int. Ed.* **2011**, *50*, 7238−7266.
(39) Gloaguen, F.; Rauchfuss, T. B. *Chem. Soc. Rev.* **2009**, *38*, 100.
(40) Barton, B. E.; Olsen, M. T.; Rauchfuss, T. B. *Curr. Opin. Biotechnol.* **2010**, *21*, 292−297.
(41) Felton, G. A. N.; Mebi, C. A.; Petro, B. J.; Vannucci, A. K.; Evans, D. H.; Glass, R. S.; Lichtenberger, D. L. *J. Organomet. Chem.* **2009**, *694*, 2681−2699.
(42) Losse, S.; Vos, J. G.; Rau, S. *Coord. Chem. Rev.* **2010**, *254*, 2492−2504.
(43) Fisher, B.; Eisenberg, R. *J. Am. Chem. Soc.* **1980**, *102*, 7361−7363.
(44) Brown, G. M.; Brunschwig, B. S.; Creutz, C.; Endicott, J. F.; Sutin, N. *J. Am. Chem. Soc.* **1979**, *101*, 1298−1300.
(45) Krishnan, C. V.; Sutin, N. *J. Am. Chem. Soc.* **1981**, *103*, 2141−2142.
(46) Krishnan, C. V.; Brunschwig, B. S.; Creutz, C.; Sutin, N. *J. Am. Chem. Soc.* **1985**, *107*, 2005−2015.
(47) Creutz, C.; Sutin, N. *Coord. Chem. Rev.* **1985**, *64*, 321−341.
(48) McNamara, W. R.; Han, Z.; Alperin, P. J.; Brennessel, W. W.; Holland, P. L.; Eisenberg, R. *J. Am. Chem. Soc.* **2011**, *133*, 15368−15371.
(49) Natali, M.; Luisa, A.; Iengo, E.; Scandola, F. *Chem. Commun.* **2014**, *50*, 1842−1844.
(50) Kellett, R. M.; Spiro, T. G. *Inorg. Chem.* **1985**, *24*, 2373−2377.




DOI: 10.1021/ic502591a
*Inorg. Chem.* 2015, 54, 646−657

(51) Varma, S.; Castillo, C. E.; Stoll, T.; Fortage, J.; Blackman, A. G.; Molton, F.; Deronzier, A.; Collomb, M.-N. *Phys. Chem. Chem. Phys.* **2013**, *15*, 17544−17552.
(52) Stubbert, B. D.; Peters, J. C.; Gray, H. B. *J. Am. Chem. Soc.* **2011**, *133*, 18070−18073.
(53) Chen, L.; Wang, M.; Han, K.; Zhang, P.; Gloaguen, F.; Sun, L. *Energy Environ. Sci.* **2014**, *7*, 329.
(54) Jacobsen, G. M.; Yang, J. Y.; Twamley, B.; Wilson, A. D.; Bullock, R. M.; DuBois, M. R.; DuBois, D. L. *Energy Environ. Sci.* **2008**, *1*, 167.
(55) Zhang, P.; Jacques, P.-A.; Chavarot-Kerlidou, M.; Wang, M.; Sun, L.; Fontecave, M.; Artero, V. *Inorg. Chem.* **2012**, *51*, 2115−2120.
(56) Probst, B.; Rodenberg, A.; Guttentag, M.; Hamm, P.; Alberto, R. *Inorg. Chem.* **2010**, *49*, 6453−6460.
(57) Probst, B.; Guttentag, M.; Rodenberg, A.; Hamm, P.; Alberto, R. *Inorg. Chem.* **2011**, *50*, 3404−3412.
(58) McCrory, C. C. L.; Uyeda, C.; Peters, J. C. *J. Am. Chem. Soc.* **2012**, *134*, 3164−3170.
(59) Hu, X.; Brunschwig, B. S.; Peters, J. C. *J. Am. Chem. Soc.* **2007**, *129*, 8988−8998.
(60) Hu, X.; Cossairt, B. M.; Brunschwig, B. S.; Lewis, N. S.; Peters, J. C. *Chem. Commun.* **2005**, 4723−4725.
(61) Du, P.; Schneider, J.; Luo, G.; Brennessel, W. W.; Eisenberg, R. *Inorg. Chem.* **2009**, *48*, 4952−4962.
(62) McCormick, T. M.; Han, Z.; Weinberg, D. J.; Brennessel, W. W.; Holland, P. L.; Eisenberg, R. *Inorg. Chem.* **2011**, *50*, 10660−10666.
(63) McCormick, T. M.; Calitree, B. D.; Orchard, A.; Kraut, N. D.; Bright, F. V.; Detty, M. R.; Eisenberg, R. *J. Am. Chem. Soc.* **2010**, *132*, 15480−15483.
(64) Lakadamyali, F.; Reisner, E. *Chem. Commun.* **2011**, *47*, 1695−1697.
(65) Wakerley, D. W.; Reisner, E. *Phys. Chem. Chem. Phys.* **2014**, *16*, 5739−5746.
(66) Razavet, M.; Artero, V.; Fontecave, M. *Inorg. Chem.* **2005**, *44*, 4786−4795.
(67) Bigi, J. P.; Hanna, T. E.; Harman, W. H.; Chang, A.; Chang, C. J. *Chem. Commun.* **2010**, *46*, 958−960.
(68) Sun, Y.; Bigi, J. P.; Piro, N. A.; Tang, M. L.; Long, J. R.; Chang, C. J. *J. Am. Chem. Soc.* **2011**, *133*, 9212−9215.
(69) Sun, Y.; Sun, J.; Long, J. R.; Yang, P.; Chang, C. J. *Chem. Sci.* **2013**, *4*, 118−124.
(70) Nippe, M.; Khnayzer, R. S.; Panetier, J. A.; Zee, D. Z.; Olaiya, B. S.; Head-Gordon, M.; Chang, C. J.; Castellano, F. N.; Long, J. R. *Chem. Sci.* **2013**, *4*, 3934−3945.
(71) Leung, C.-F.; Ng, S.-M.; Ko, C.-C.; Man, W.-L.; Wu, J.; Chen, L.; Lau, T.-C. *Energy Environ. Sci.* **2012**, *5*, 7903−7907.
(72) Mandal, S.; Shikano, S.; Yamada, Y.; Lee, Y.-M.; Nam, W.; Llobet, A.; Fukuzumi, S. *J. Am. Chem. Soc.* **2013**, *135*, 15294−15297.
(73) Singh, W. M.; Mirmohades, M.; Jane, R. T.; White, T. A.; Hammarström, L.; Thapper, A.; Lomoth, R.; Ott, S. *Chem. Commun.* **2013**, *49*, 8638−8640.
(74) Singh, W. M.; Baine, T.; Kudo, S.; Tian, S.; Ma, X. A. N.; Zhou, H.; DeYonker, N. J.; Pham, T. C.; Bollinger, J. C.; Baker, D. L.; Yan, B.; Webster, C. E.; Zhao, X. *Angew. Chem.* **2012**, *124*, 6043−6046.
(75) Zhang, P.; Wang, M.; Gloaguen, F.; Chen, L.; Quentel, F.; Sun, L. *Chem. Commun.* **2013**, *49*, 9455−9457.
(76) Guttentag, M.; Rodenberg, A.; Bachmann, C.; Senn, A.; Hamm, P.; Alberto, R. *Dalton Trans.* **2013**, *42*, 334−337.
(77) Bachmann, C.; Guttentag, M.; Spingler, B.; Alberto, R. *Inorg. Chem.* **2013**, *52*, 6055−6061.
(78) Guttentag, M.; Rodenberg, A.; Kopelent, R.; Probst, B.; Buchwalder, C.; Brandstätter, M.; Hamm, P.; Alberto, R. *Eur. J. Inorg. Chem.* **2012**, *2012*, 59−64.
(79) Khnayzer, R. S.; Thoi, V. S.; Nippe, M.; King, A. E.; Jurss, J. W.; El Roz, K. A.; Long, J. R.; Chang, C. J.; Castellano, F. N. *Energy Environ. Sci.* **2014**, *7*, 1477−1488.
(80) Bachmann, C.; Probst, B.; Guttentag, M.; Alberto, R. *Chem. Commun.* **2014**, *50*, 6737−6739.
(81) Marinescu, S. C.; Winkler, J. R.; Gray, H. B. *Proc. Natl. Acad. Sci. U.S.A.* **2012**, *109*, 15127−15131.
(82) Dempsey, J. L.; Brunschwig, B. S.; Winkler, J. R.; Gray, H. B. *Acc. Chem. Res.* **2009**, *42*, 1995−2004.
(83) Chao, T.-H.; Espenson, J. H. *J. Am. Chem. Soc.* **1978**, *100*, 129−133.
(84) Dempsey, J. L.; Winkler, J. R.; Gray, H. B. *J. Am. Chem. Soc.* **2010**, *132*, 16774−16776.
(85) Bhattacharjee, A.; Andreiadis, E. S.; Chavarot-Kerlidou, M.; Fontecave, M.; Field, M. J.; Artero, V. *Chem.—Eur. J.* **2013**, *19*, 15166−15174.
(86) Muckerman, J. T.; Fujita, E. *Chem. Commun.* **2011**, *47*, 12456−12458.
(87) Solis, B. H.; Hammes-Schiffer, S. *Inorg. Chem.* **2011**, *50*, 11252−11262.
(88) Tinker, L. L.; McDaniel, N. D.; Bernhard, S. *J. Mater. Chem.* **2009**, *19*, 3328−3337.
(89) Hoffman, M. Z. *J. Phys. Chem.* **1988**, *92*, 3458−3464.
(90) Sun, H.; Hoffman, M. Z. *J. Phys. Chem.* **1994**, *98*, 11719−11726.
(91) Fukuzumi, S.; Kobayashi, T.; Suenobu, T. *Angew. Chem., Int. Ed.* **2011**, *50*, 728−731.
(92) Sutin, N. *J. Photochem.* **1979**, *10*, 19−40.
(93) Macartney, D. H.; Sutin, N. *Inorg. Chim. Acta* **1983**, *74*, 221−228.
(94) DeLaive, P. J.; Foreman, T. K.; Giannotti, C.; Whitten, D. G. *J. Am. Chem. Soc.* **1980**, *102*, 5627−5631.
(95) Neshvad, G.; Hoffman, M. Z. *J. Phys. Chem.* **1989**, *93*, 2445−2452.
(96) Chan, S.-F.; Chou, M.; Creutz, C.; Matsubara, T.; Sutin, N. *J. Am. Chem. Soc.* **1981**, *103*, 369−379.
(97) Kalyanasundaram, K.; Kiwi, J.; Grätzel, M. *Helv. Chim. Acta* **1978**, *61*, 2720−2730.
(98) Sutin, N.; Creutz, C.; Fujita, E. *Comments Inorg. Chem.* **1997**, *19*, 67−92.
(99) Shan, B.; Baine, T.; Ma, X. A. N.; Zhao, X.; Schmehl, R. H. *Inorg. Chem.* **2013**, *52*, 4853−4859.
(100) Fischer, H.; Radom, L. *Angew. Chem., Int. Ed.* **2001**, *40*, 1340−1371.
(101) Neta, P. *Adv. Phys. Org. Chem.* **1976**, *12*, 223−297.
(102) Wagner, P. J.; Zhang, Y.; Puchalski, A. E. *J. Phys. Chem.* **1993**, *97*, 13368−13374.
(103) Nazran, A. S.; Griller, D. *J. Am. Chem. Soc.* **1983**, *105*, 1970−1971.
(104) Turro, N. J.; Lei, X.; Jockusch, S.; Li, W.; Liu, Z.; Abrams, L.; Ottaviani, M. F. *J. Org. Chem.* **2002**, *67*, 2606−2618.
(105) Schuh, H.-H.; Fischer, H. *Helv. Chim. Acta* **1978**, *61*, 2130−2164.
(106) Neta, P.; Grodkowski, J.; Ross, A. B. *J. Phys. Chem. Ref. Data* **1996**, *25*, 709−1050.
(107) Gibian, M. J.; Corley, R. C. *Chem. Rev.* **1973**, *73*, 441−464.
(108) Kelley, R. D.; Klein, R. *J. Phys. Chem.* **1974**, *78*, 1586−1595.
(109) Chan, S. J.; Howe, A. G.; Hook, J. M.; Harper, J. B. *Magn. Reson. Chem.* **2009**, *47*, 342−347.
(110) Orpen, A. G.; Brammer, L.; Allen, F. H.; Kennard, O.; Watson, D. G.; Taylor, R. *J. Chem. Soc., Dalton Trans.* **1989**, S1−S83.
(111) Wayner, D. D. M.; McPhee, D. J.; Griller, D. *J. Am. Chem. Soc.* **1988**, *110*, 132−137.
(112) King, A. E.; Surendranath, Y.; Piro, N. A.; Bigi, J. P.; Long, J. R.; Chang, C. J. *Chem. Sci.* **2013**, *4*, 1578.
(113) Hori, H.; Ishihara, J.; Koike, K.; Takeuchi, K.; Ibusuki, T.; Ishitani, O. *J. Photochem. Photobiol., A* **1999**, *120*, 119−124.
(114) Georgopoulos, M.; Hoffman, M. Z. *J. Phys. Chem.* **1991**, *95*, 7717−7721.
(115) Kutal, C.; Corbin, A. J.; Ferraudi, G. *Organometallics* **1987**, *6*, 553−557.
(116) Burkey, T. J.; Castelhano, A. L.; Griller, D.; Lossing, F. P. *J. Am. Chem. Soc.* **1983**, *105*, 4701−4703.
(117) Griller, D.; Lossing, F. P. *J. Am. Chem. Soc.* **1981**, *103*, 1586−1587.


DOI: 10.1021/ic502591a
*Inorg. Chem.* 2015, 54, 646−657

(118) Kirch, M.; Lehn, J.-M.; Sauvage, J.-P. *Helv. Chim. Acta* **1979**, *62*, 1345−1384.
(119) Du, P.; Schneider, J.; Jarosz, P.; Eisenberg, R. *J. Am. Chem. Soc.* **2006**, *128*, 7726−7727.
(120) Wayner, D. D. M.; Dannenberg, J. J.; Griller, D. *Chem. Phys. Lett.* **1986**, *131*, 189−191.
(121) Watanabe, T.; Honda, K. *J. Phys. Chem.* **1982**, *86*, 2617−2619.
(122) Mann, K. R.; Gordon, J. G., II; Gray, H. B. *J. Am. Chem. Soc.* **1975**, *97*, 3553−3555.
(123) Marino, N.; Fazen, C. H.; Blakemore, J. D.; Incarvito, C. D.; Hazari, N.; Doyle, R. P. *Inorg. Chem.* **2011**, *50*, 2507−2520.
(124) Bercaw, J. E.; Durrell, A. C.; Gray, H. B.; Green, J. C.; Hazari, N.; Labinger, J. A.; Winkler, J. R. *Inorg. Chem.* **2010**, *49*, 1801−1810.
(125) Connick, W. B.; Marsh, R. E.; Schaefer, W. P.; Gray, H. B. *Inorg. Chem.* **1997**, *36*, 913−922.
(126) Mann, K. R.; Gray, H. B. In *Inorganic Compounds with Unusual Properties-II*; King, R. B., Ed.; Advances in Chemistry; American Chemical Society: Washington, DC, 1979; Vol. *173*, pp 225−235.
(127) Rice, S. F.; Milder, S. J.; Gray, H. B.; Goldbeck, R. A.; Kliger, D. S. *Coord. Chem. Rev.* **1982**, *43*, 349−354.
(128) Carr, N.; Crossley, J. G.; Dent, A. J.; Gouge, J. R.; Greaves, G. N.; Jarrett, P. S.; Orpen, A. G. *J. Chem. Soc., Chem. Commun.* **1990**, 1369−1371.
(129) Novoa, J. J.; Aullón, G.; Alemany, P.; Alvarez, S. *J. Am. Chem. Soc.* **1995**, *117*, 7169−7171.
(130) Smith, D. C.; Gray, H. B. *Coord. Chem. Rev.* **1990**, *100*, 169−181.
(131) Rice, S. F.; Gray, H. B. *J. Am. Chem. Soc.* **1983**, *105*, 4571−4575.
(132) Aullón, G.; Alemany, P.; Alvarez, S. *Inorg. Chem.* **1996**, *35*, 5061−5067.
(133) Schrauzer, G. N. *Angew. Chem., Int. Ed. Engl.* **1976**, *15*, 417−426.
(134) Toscano, P. J.; Marzilli, L. G. In *Progress in Inorganic Chemistry*; Lippard, S. J., Ed.; John Wiley & Sons: New York, 1984; pp 105−204.
(135) Gupta, B. D.; Roy, S. *Inorg. Chim. Acta* **1988**, *146*, 209−221.
(136) Zhou, D.-L.; Tinembart, O.; Scheffold, R.; Walder, L. *Helv. Chim. Acta* **1990**, *73*, 2225−2241.
(137) Lexa, D.; Saveant, J. M. *Acc. Chem. Res.* **1983**, *16*, 235−243.
(138) Schrauzer, G. N.; Windgassen, R. J. *Nature* **1967**, *214*, 492. Aniline and formaldehyde react in the presence of $H_2$ as reductant with cobaloxime(II). The resulting $\alpha$-aminoalkyl cobalt complex is formed quantitatively in methanol as solvent and can be isolated. Hydrolysis in acidic solution gives back the educts and $Co^{II}$, while only a small fraction of *N*-methylaniline is formed due to reductive cleavage of the Co−C bond. Although it is not mentioned, $Co^{I}$ formed upon hydrolysis most likely reacts back to $Co^{II}$ via proton reduction under the acidic conditions applied. An indication for this is the observation that the thermal decomposition of the $\alpha$-aminoalkyl cobalt complex in pyridine as solvent produced *N*-methylaniline in close to stoichiometric amounts.
(139) Wiesenburg, D. A.; Guinasso, N. L., Jr. *J. Chem. Eng. Data* **1979**, *24*, 356−360.
(140) Grimme, S. *J. Chem. Phys.* **2006**, *124*, 034108.
(141) Grimme, S. *J. Comput. Chem.* **2006**, *27*, 1787−1799.
(142) Weigend, F.; Ahlrichs, R. *Phys. Chem. Chem. Phys.* **2005**, *7*, 3297−3305.
(143) Baldridge, K.; Klamt, A. *J. Chem. Phys.* **1997**, *106*, 6622−6633.
(144) Klamt, A.; Schüürmann, G. *J. Chem. Soc., Perkin Trans. 2* **1993**, 799−805.
(145) Chai, J.-D.; Head-Gordon, M. *Phys. Chem. Chem. Phys.* **2008**, *10*, 6615−6620.


DOI: 10.1021/ic502591a
*Inorg. Chem.* 2015, 54, 646−657